

Supported by



Accepted Article

Title: Reductive Formylation of Nitroarenes using HCOOH over Bimetallic C-N Framework Derived from the Integration of MOF and COF

Authors: Rajendra Srivastava and Ashish Kumar Kar

This manuscript has been accepted after peer review and appears as an Accepted Article online prior to editing, proofing, and formal publication of the final Version of Record (VoR). This work is currently citable by using the Digital Object Identifier (DOI) given below. The VoR will be published online in Early View as soon as possible and may be different to this Accepted Article as a result of editing. Readers should obtain the VoR from the journal website shown below when it is published to ensure accuracy of information. The authors are responsible for the content of this Accepted Article.

To be cited as: *ChemCatChem* 10.1002/cctc.202100412

Link to VoR: <https://doi.org/10.1002/cctc.202100412>

FULL PAPER

Reductive Formylation of Nitroarenes using HCOOH over Bimetallic C-N Framework Derived from the Integration of MOF and COF

Ashish Kumar Kar^[a] and Rajendra Srivastava^{*[a]}

[a] Mr. Ashish Kumar Kar, Dr. Rajendra Srivastava
Catalysis Research Laboratory, Department of Chemistry,
Indian Institute of Technology Ropar,
Rupnagar-140001, Punjab, India.
E-mail: rajendra@iitpr.ac.in

Supporting information for this article is given via a link at the end of the document. ((Please delete this text if not appropriate))

Abstract: CoZn embedded C-N framework is prepared by the carbonization of CoZn containing MOF integrated with COF porous architecture in Ar atmosphere. The graphitic nature of porous carbon is confirmed from Raman analysis. The porosity and nanostructure information are retrieved from N₂-sorption and transmission electron microscopic analysis, respectively. The incorporation of different metals & their oxidation states and types of nitrogen present in the C-N framework are confirmed from X-ray photoelectron spectroscopy. The basicity of the materials is determined from a CO₂-temperature programmed desorption. ZnCo embedded C-N framework exhibits excellent activity in the selective reductive formylation using HCOOH. For comparison, more than 15 materials are prepared, and their activities are compared. Several control experiments are performed to establish a structure-activity relation. The recycling experiment, hot-filtration test, and poisoning experiment demonstrate the metal embedded porous C-N framework's recyclability and stability. A reaction mechanism for the reductive N-formylation of nitroaromatics is presented based on structure-activity relationship, control reactions, and physicochemical characterizations. The development of interesting MOF-COF-derived metal nanoclusters embedded C-N framework for selective reductive formylation of nitroaromatics using formic acid will be highly attractive to catalysis researchers and industrialists.

Introduction

The current energy demands are satisfied through non-renewable resources threatening to maintain the ecological system suitable for human survival. Thus, it has become imperative to develop an environment-benign energy conversion process to meet global energy demand.^[1-2] Hydrogen is one of the most abundant elements on the earth. However, it is not found in the troposphere in large concentrations in the gaseous form. It is present in the combined state in various renewable and non-renewable resources. Hydrogen is a key precursor for the production of a large number of bulk and commodities chemicals.^[3-5] Moreover, hydrogen-based sustainable energy conversion processes such as fuel cells can serve the energy demands to a greater extent.^[6] No doubt, hydrogen is a clean energy source and one of the best options for zero-emission energy carriers. However, in conventional practice, H₂ is mainly produced by the steam reforming process, by which a large excess of CO₂ (almost three times that of H₂) is emitted, which is a real threat to global warming.^[7-8] The benign environmental process for H₂ production is photocatalytic water splitting or water electrolysis that is under the growing stage and is yet to

be implemented across the world.^[9-10] The significant bottlenecks of this development are expensive experimental setup and low efficiency. Therefore, it is beneficial to carry out chemical synthesis without the direct use of hydrogen gas. Moreover, the use of H₂ gas requires a particular leak-proof reaction setup. Thus, transfer hydrogenation is employed, which is a more user-friendly, facile, economical, and sustainable method. In general, transfer hydrogenation uses alcohol as a transfer hydrogen source.^[11-12] However, these alcohols (such as methanol) are also produced using H₂ as a reactant.¹³ Various other hydrogenation sources such as hydrazine hydrate and sodium borohydride are non-economical and non-eco-friendly with poor reversibility of hydrogen.^[14-15] Thus, it is essential to develop a catalytic transfer hydrogenation process involving renewable hydrogenation sources such as formic acid.^[16-17] Formic acid is produced by biomass.^[16,18] Moreover, formic acid (FA) can also be used as a formylating source.^[17,19] Herein, FA is employed as an H₂ and formylating source for the reductive formylation of nitrobenzene (NB) in a direct one-step process.

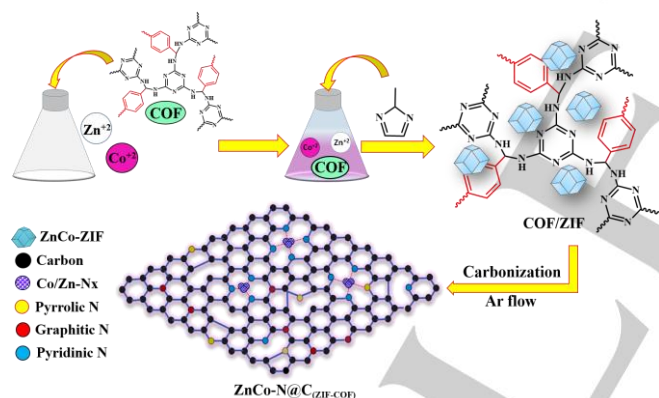
Aryl amines and N-Aryl formamides are important intermediates and have broad application in polymers, pharmaceuticals, agrochemicals, dyes, and fragrances.^[20-22] Moreover, their inherent property for being a potential candidate to synthesize various biologically active scaffolds cannot be ruled out. Typical routes for the synthesis of N-aryl formamides include direct formylation of aniline and nitrobenzene's reductive formylation.^[23-24] The former is more facile and involves a straightforward synthetic route for the synthesis of N-aryl formamides. However, the later synthetic method involves a more challenging pathway when it is carried out in one-pot. In this work, the challenging reductive N-formylation of nitrobenzene to N-aryl formamides is demonstrated via a sustainable catalytic approach using formic acid as a hydrogen and formylating source.

The conversion of formic acid to H₂ and/or CO requires a suitable metal center.^[25-27] The metal should be stabilized in a porous matrix to not leach out during the reaction. Further, the adsorption of formic acid requires basic support.^[17] In this reaction, one should have a suitable N doping along with a high surface area for the concomitant adsorption of formic acid and reactant. Thus, a high surface area porous N-doped carbon material is a key feature. In general, N-doped carbon materials are built with pyrrolic, pyridinic, and graphitic N-units.^[17,28] Higher N contents are not always dominant factors for catalysis, but the N environment is an important factor responsible for providing optimum metal stability and reactivity.^[28] Metal or metal oxide-containing porous carbon or N-doped carbon materials can be prepared using a metal-organic framework (MOF).^[29-31] It is

FULL PAPER

possible to synthesize metal-containing porous N doped carbon materials by directly reacting carbon and nitrogen-bearing sources and metal precursors.^[17] However, MOF-derived metal-containing N-doped porous carbon is more attractive and active due to the pre-existing bonding of metal with MOF framework that provides high stability, highly dispersed and small size metal clusters, suitable for excellent catalysis.^[29,30] Covalent organic framework provides an ordered N-doped carbon framework with better textural properties than other N-containing carbon sources providing C-N framework.^[32] It is possible to enhance the N-doping with a suitable N environment and textural properties by integrating MOF with other N-containing porous materials. Only a handful of work in this direction has been done.^[33-35] Thus, it is interesting to develop metal nanoclusters containing N-doped carbon materials by integrating MOF and other C-N frameworks.

This study demonstrates the catalytic reductive formylation of nitrobenzene (NB) in a direct one-step process with formic acid using the ZnCo-N doped porous carbon-nitrogen framework. ZnCo co-doped porous carbon-nitrogen framework is prepared by carbonizing Co-Zn zeolitic imidazole framework (ZIF) grown over the porous covalent organic framework. Several mono-metallic and bi-metallic C-N frameworks are also prepared and investigated in this reaction. A suitable composition of Co and Zn in the C-N framework is required to achieve high activity and selectivity for the reductive formylated product. The development of a tunable metal composition with a particular C-N framework, exhibiting excellent activity for the challenging one-pot reductive formylation of nitrobenzene, will be highly attractive for catalysis and materials synthesis prospective.



Scheme 1. Schematic presentation for the synthesis of Zn-Co doped porous carbon-nitrogen framework.

Results and Discussion

The schematic presentation for the synthesis of the Zn-Co co-doped porous carbon-nitrogen framework is presented in Scheme 1. First, a covalent organic framework (COF) was prepared by condensation of melamine and terephthalaldehyde. Then ZnCo-ZIF precursors (Zn & Co precursors and 2-methylimidazole) were added to the as-synthesized COF to prepare ZnCo-ZIF integrated with the COF framework. The resultant material was carbonized under a specific condition described in the experimental section to obtain ZnCo-N@C_(ZIF-COF) catalyst. During the carbonization process, the ZIF framework was integrated with the COF framework and resulted in the formation of an N-doped porous carbon framework embedding metal

species. Two more bimetallic catalysts were prepared to understand the structural-activity relationship in the reductive N-formylation of nitrobenzene. ZnCo-ZIF precursors were added to melamine to prepare ZnCo-ZIF integrated with melamine. The resultant material was carbonized to obtain ZnCo-N@C_(ZIF-MEL) catalyst. ZnCo-ZIF was carbonized to obtain ZnCo-N@C_(ZIF). Zn-ZIF and Co-ZIF were carbonized to obtain Zn-N@C_(ZIF) and Co-N@C_(ZIF), respectively.

Physicochemical Characterization

The structure of COF was confirmed by FT-IR and Solid-state ¹³C CP MAS NMR. The FT-IR spectra of terephthalaldehyde, melamine, and COF are plotted (Figure S1). Melamine exhibits characteristics sharp peaks at 3468 cm⁻¹, and 3419 cm⁻¹ correspondings to NH₂-stretching vibrations and peak at 1649 cm⁻¹ correspond to NH₂-deformation mode. Terephthalaldehyde exhibits characteristics peak at 2865 cm⁻¹ and 1687 cm⁻¹ corresponding to aldehydic C-H stretching and carbonyl group, respectively. The above-mentioned FT-IR peaks are absent in the COF material suggesting the complete condensation of -NH₂ of melamine and -CHO of terephthalaldehyde. COF shows triazine units' presence due to FT-IR peaks at 1543 cm⁻¹ and 1479 cm⁻¹ corresponding to C=N, which confirm the presence of melamine units in COF structure. No peak at 1600 cm⁻¹ is observed, suggesting that the COF framework is built with amina moiety (HN-C-NH).^[36] ¹³C CP MAS NMR also confirmed the formation of the COF framework (Figure S2). A peak at 166 ppm corresponds to triazine units, peaks at 135 ppm and 129 ppm correspond to aromatic carbons, and 54 ppm corresponds to amina carbon.^[36] No peaks at 190 ppm and 160 ppm confirm the absence of the free aldehyde group of terephthalaldehyde and imine bonds, respectively. Field-emission scanning electron microscopy (FE-SEM) analysis shows that COF exhibits aggregated morphology, whereas ZIF exhibits a rhomboid dodecahedron morphology (Figure S3). The composite material shows that the ZnCo-ZIF is uniformly dispersed with the COF matrix.

All the synthesized C-N catalysts exhibit a broad XRD peak in the range of 15-30° (Figure 1A). The diffraction maxima of the broad reflection appear close to 25°, which are marginally deviated from the C (001) reflection known for a carbon material.^[37] This suggests that the synthesized catalysts are graphitic.^[37] Diffraction peaks at 43.3° and 51.3° are observed for all the ZnCo-N@C catalysts indicating the presence of metallic Co species.¹⁷ A weak diffraction peak around 36.5° is observed for the ZnCo-N@C_(ZIF), suggesting the presence of CoO in the ZnCo-N@C_(ZIF) catalyst. Moreover, a weaker diffraction peak around 36.5° is observed in ZnCo-N@C_(ZIF-MEL) than ZnCo-N@C_(ZIF) (Figure 1A). An exceptionally weak diffraction peak could be observed around 36.5° in ZnCo-N@C_(ZIF-COF). Based on this investigation, it can be concluded that ZIF-COF integrated carbonized framework provides stability to Co and Zn species in a highly dispersed state and prevent them from oxidation leading to produce metal oxide phase. The XRD patterns of monometallic MOF, bi-metallic MOF, COF, and other materials prepared in this study are provided in the supporting information section (Figure S4).

Raman analysis provides information about the nature of carbon present in the catalyst. The Peaks at 1358 cm⁻¹ and 1589 cm⁻¹ in the Raman spectrum of various ZnCo-N@C catalysts

FULL PAPER

correspond to the D-band and G-band of graphitic carbon (Figure 1B).^[31] The ratio of I_D/I_G defines the surface defect degree of the carbon framework. The I_D/I_G values obtained for the $\text{ZnCo-N@C}_{(\text{ZIF-MEL})}$, $\text{ZnCo-N@C}_{(\text{ZIF-COF})}$, and $\text{ZnCo-N@C}_{(\text{ZIF})}$ are 1.05, 1.01, and 0.99, respectively. Vibration peaks observed in the range of $300\text{--}500\text{ cm}^{-1}$ correspond to the Zn/Co-O/N species present in the $\text{ZnCo-N@C}_{(\text{ZIF-COF})}$ catalyst (Figure 1B).^[17] The graphitic nature of the various materials prepared in this study suggests that they are conducting and facilitating the electron transfer between the reactant and catalyst surface, promoting the decomposition of HCOOH to CO/H_2 .

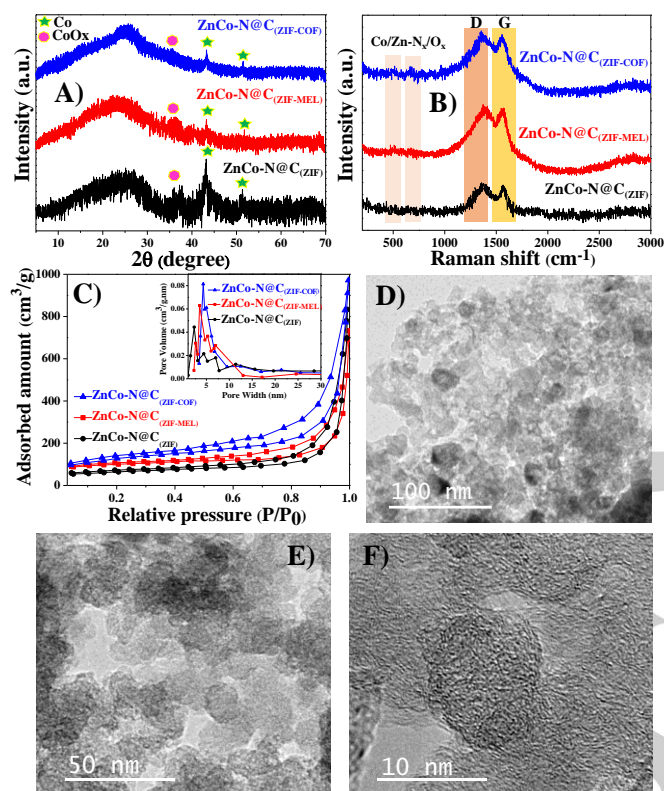


Figure 1. (A) Powder XRD patterns, (B) Raman spectra, (C) N_2 -sorption isotherms of various ZnCo-N@C catalyst. (D-F) TEM images of $\text{ZnCo-N@C}_{(\text{ZIF-COF})}$.

The N_2 -sorption analysis was carried out to determine the textural properties of the ZnCo-N@C catalysts. All three catalysts exhibit a type-IV isotherm and H3 hysteresis loop (Figure 1C). A steady increase in the N_2 -adsorption volume is observed in the range of 0 to 0.8 (P/P_0), followed by a steep increase in the N_2 -adsorption volume representing interparticle porosity. The inset of Figure 1C shows the pore size distribution obtained from the BJH method. The surface area of the materials follows the order $\text{ZnCo-N@C}_{(\text{ZIF-COF})} > \text{ZnCo-N@C}_{(\text{ZIF})} > \text{ZnCo-N@C}_{(\text{ZIF-MEL})}$, indicating that MOF-COF entangled material provides better surface area (Table 1).

Table 1. Textural properties of various ZnCo-N@C catalysts.

Catalyst	S_{BET} (m^2/g)	Pore diameter (nm)	Pore volume (cm^3/g)	S_{ext} (m^2/g)
$\text{ZnCo-N@C}_{(\text{ZIF})}$	601.3	2.28	0.91	391.8
$\text{ZnCo-N@C}_{(\text{ZIF-COF})}$	684.6	4.36	2.1	409.7
$\text{ZnCo-N@C}_{(\text{ZIF-MEL})}$	549.5	3.60	1.78	349.1

$\text{ZnCo-N@C}_{(\text{ZIF})}$	601.3	2.28	0.91	391.8
$\text{ZnCo-N@C}_{(\text{ZIF-COF})}$	684.6	4.36	2.1	409.7
$\text{ZnCo-N@C}_{(\text{ZIF-MEL})}$	549.5	3.60	1.78	349.1

TEM and high-resolution TEM (HRTEM) images show aggregated porous carbon nanostructure present in $\text{ZnCo-N@C}_{(\text{ZIF-COF})}$ (Figure 1D-F). HRTEM image shows regions with lattice fringes corresponding to graphitic carbon present in the material, consistent with the Raman analysis. Cobalt or Zn nanoparticles are not visible in the TEM images suggesting that the metal nanoclusters are present in a highly dispersed state in the material. EDAX analysis and elemental mapping indicate the uniform distribution of Co and Zn metals in a porous C-N framework (Figure S5). The low concentration of Zn compared to Co in the elemental mapping confirms the Zn's evaporation during the carbonization step.

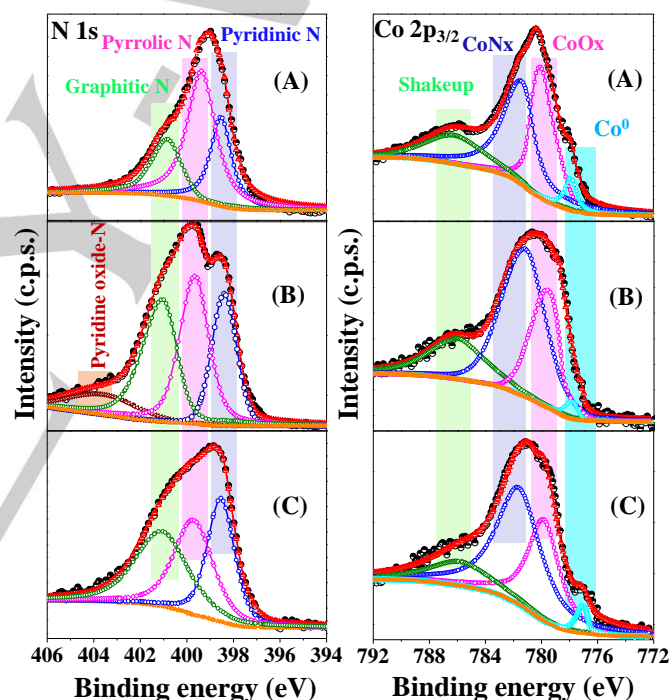


Figure 2. The high resolution XPS spectra of N 1s and Co 2p present in (A) $\text{ZnCo-N@C}_{(\text{ZIF-COF})}$, (B) $\text{ZnCo-N@C}_{(\text{ZIF-MEL})}$, and (C) $\text{ZnCo-N@C}_{(\text{ZIF})}$.

The surface elemental compositions and their oxidation states were evaluated from XPS analysis. The surface survey analysis confirms Zn, Co, N, O, and C in the synthesized catalyst (Figure S6). The details of the surface elemental compositions are presented in Table S1. The Zn contents in the materials are smaller than the input value. This is due to the volatile nature of Zn, which escapes from the materials during the carbonization process.^[35, 37] The surface Zn has more escaping tendency than the Zn incorporated in the C-N framework. The high-resolution XPS spectra of Zn 2p show two deconvoluted peaks at 1044.7 eV and 1021.5 eV corresponding to the Zn $2p_{1/2}$ and Zn $2p_{3/2}$ of Zn-Nx species (Figure S7).^[38] The

FULL PAPER

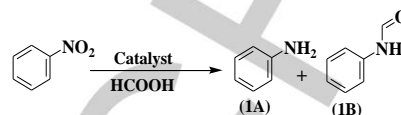
high-resolution XPS spectra of the Co 2p_{3/2} exhibits four peaks at the binding energy of 778.2 eV for Co(0), 779.4 eV for CoO_x, 781.6 eV for CoN_x, and a shakeup peak at 786.1 eV (Figure 2).^[17] A low area deconvoluted profile with a peak maximum at 778.2 eV indicates that the low concentration of metallic Co(0) present in ZnCo-N@C_(ZIF-COF) and ZnCo-N@C_(ZIF-MEL) catalysts. Co nanoclusters are bonded and stabilized through various types of "N" species present in the material. The coordination between "N" species and Co results in a partial electron transfer from Co to N atoms, which create a positive charge on Co and form Co-N_x species occurring at a higher binding energy of 781.6.^[39-41] Furthermore, the surface Co nanoclusters are highly sensitive to the aerobic atmosphere and form a low concentration of CoO_x phase, which is observed at 779.4 eV in the deconvolution spectrum.^[42] The deconvoluted N 1s XPS spectra suggest the occurrence of pyridinic N, pyrrolic N, and graphitic N at 398.2 eV, 399.5 eV, and 401.2 eV, respectively (Figure 2).^[17] An additional peak appears at 404.1 eV in ZnCo-N@C_(ZIF-MEL) suggests the presence of pyridine N-oxide.^[17] The presence of different nitrogen environments in all three catalysts suggests the successful entrapment of metallic (Co and Zn) constituents in the materials. Moreover, the XPS spectrum of C1s indicates the presence of C=C in all three catalysts (Figure S8). The carbonized structure of ZIF-COF contains a suitable N environment (pyrrolic N, pyridine N) for stabilizing different Co species. However, some Co species (especially surface Co species) could not be prevented from oxidation in aerobic conditions. Hence the occurrence of CoO_x can be observed in the XRD and XPS analysis.

Evaluation of catalytic activity

The one-pot direct N-formylation of the -NO₂ of NB to the corresponding N-formyl aniline (AN) using formic acid as the reducing and formylating source is presented here. The activation of formic acid takes place via its adsorption on the suitable metal sites. The basic nature of C-N framework is ideal for formic acid adsorption.^[17] Besides, the high surface area and porosity are essential for the adsorption of reactant molecules and entrapment of metal species in a highly dispersed state. Zn is known to facilitate the adsorption and decomposition of formic acid.^[43, 44] In contrast, the Co is known for forming H₂ + CO₂ or/and CO + H₂O from the formic acid.^[26,45-46] Thus, the bimetallic constituent of the catalyst is advantageous for utilizing the formic acid in the one-pot reductive formylation of NB. The reductive formylation depends on the composition of H₂ + CO₂ and CO + H₂O, whose generation depends on several experimental factors, including the catalyst's chemical compositions. Thus, it is highly interesting to develop a catalyst to generate H₂ and CO in a suitable ratio to form the desired N-formylated product. Herein, various ZnCo-N@C catalysts are employed for the reductive formylation of the NB and its derivatives to its corresponding N-formyl AN derivatives. NB is chosen as a model substrate to find the best catalyst and optimized reaction conditions. No NB conversion is observed in the absence of a catalyst (Entry 1, Table 2). There is no reduced or formylated product obtained when the reaction is carried out in the absence of the formic acid but in the presence of the catalyst. Very low NB conversion is observed using ZIF-67, ZIF-8, ZnCo-ZIF, and COF catalysts (Entries 2-5, Table 2). All carbonized catalysts are active for this reaction. Co-N@C_(ZIF-67) exhibits higher NB conversion than Zn-N@C_(ZIF-8) (Compare

entries 6-7, Table 2). However, the selectivity for formanilide (1b, compare entries 6-7, Table 2) is more in Zn-N@C_(ZIF-8). Further, upon integrating MOF and COF, the resultant monometallic carbonized catalysts exhibit better NB conversion (Compare entries 6,7 with 9,10, Table 2).

Table 2. Reductive formylation of nitrobenzene using HCOOH over various catalysts prepared in this study.



Entry	Catalyst	NB Conv. (%)	Product Selectivity (%)	
			1A	1B
1	None	0	ND	ND
2	ZIF-67	3	48	52
3	ZIF-8	2	29	71
4	ZnCo-ZIF	4	20	80
5	COF	1	79	21
6	^a Zn-N@C _(ZIF-8)	26	11	89
7	^a Co-N@C _(ZIF-67)	52	55	45
8	^a ZnCo-N@C _(ZIF)	71	20	80
9	^a Zn-N@C _(ZIF-8-COF)	34	9	91
10	^a Co-N@C _(ZIF-67-COF)	69	53	47
11	^a ZnCo-N@C _(ZIF-COF)	98	14	86
12	^a Zn _{1.5} Co _{0.5} -N@C _(ZIF-COF)	96	10	89
13	^a Zn _{1.75} Co _{0.25} -N@C _(ZIF-COF)	94	9	91
14	^a Zn _{1.9} Co _{0.1} -N@C _(ZIF-COF)	71	10	90
15	Zn _{1.75} Co _{0.25} -N@C _{(ZIF-COF)973K}	41	24	76
16	Zn _{1.75} Co _{0.25} -N@C _{(ZIF-COF)1023K}	69	9	91
17	Zn _{1.75} Co _{0.25} -N@C _{(ZIF-COF)1073K}	84	38	62
18	Zn _{1.75} Co _{0.25} -N@C _{(ZIF-COF)1173K}	89	6	94
19	^a Zn _{1.75} Co _{0.25} -N@C _(ZIF-MEL)	79	14	86
20	^a Zn _{1.75} Co _{0.25} -N@C _(ZIF)	65	15	85
21	^{a,b} Zn _{1.75} Co _{0.25} -N@C _(ZIF-COF)	30	100	-

Reaction condition: Nitrobenzene (1 mmol), HCOOH (12 equiv.), catalyst (30 mg), THF (7 mL), temperature (413 K), time (8 h). ^aCarbonized at 1123 K, ^bH₂ pressure = 5 bar.

FULL PAPER

However, the formanilide selectivity is higher in the case of Zn catalyst (Compare entries 6,7 with 9,10, Table 2). Thus, the Zn and Co ratio's influence is varied to obtain higher NB conversion and formanilide selectivity. Since Zn metal drives the selectivity, therefore higher input Zn content is selected. The input ratio of Zn:Co (in wt%) is varied, and the material with $Zn_{1.75}Co_{0.25}N@C_{(ZIF-COF)}$ exhibits the best selectivity towards formanilide (compare entries 11-14, Table 2). With other compositions, either lower selectivity of the formanilide or the lower NB is observed. The influence of carbonization temperature on the catalytic activity is investigated. Better NB conversion and formanilide selectivity are obtained for the material treated as 1123 K (compare entries 13, 15-18, Table 2). $Zn_{1.75}Co_{0.25}N@C_{(ZIF-MEL)}$ and $Zn_{1.75}Co_{0.25}N@C_{(ZIF)}$ exhibit inferior activity than $Zn_{1.75}Co_{0.25}N@C_{(ZIF-COF)}$, carbonized at 1123 K (compare entries 13, 19, and 20, Table 2). When the hydrogenation of the NB is carried out in the presence of the H_2 gas, the aniline yield is only 30 % (Entry 20, Table 2). This suggests the in-situ generated $CO+H_2$ from the formic acid is responsible for this NB reductive formylation reaction. After finding the best catalyst $Zn_{1.75}Co_{0.25}N@C_{(ZIF-COF)}$ (hereafter denoted as $ZnCo-N@C_{(ZIF-COF)}$), factors influencing the product yields are investigated. The amount of catalyst is varied in the range of 20-40 mg. The best activity is achieved using 30 mg of catalyst for 1 mmol of nitrobenzene (Figure 3A). The reaction duration also plays an important role because more aniline is formed at the beginning of the reaction, subsequently reaction with CO to form the formanilide (Figure 3B). After 8 h of the reaction, the best activity is achieved. Another important parameter is the temperature because the mode of HCOOH decomposition extensively depends on the reaction temperature, which subsequently affects the formanilide selectivity. The HCOOH at elevated temperature (>393 K) preferentially decomposes under the dehydration ($HCOOH \rightarrow CO+H_2O$) pathway. Hence the chance of forming the formylated product via an indirect pathway is more (Discussed later in the mechanism section).^[45,48] Thus, the reactions are performed at four different reaction temperatures in the range of 393 K to 423 K (Figure 3C). With an increase in the temperature, formanilide selectivity increases. The best activity and formanilide selectivity are obtained at 413 K. An almost similar result is obtained when the reaction temperature is raised to 423 K. Careful inspection of data reveal that above 393 K, the rate of CO formation is increased when compared to H_2 formation. This is the reason; higher formanilide selectivity is obtained at 413 K. The activation energy obtained for this reaction is calculated to be 25.6 kJ/mole (The details can be found in the Supporting information section, Figure S9). The NB conversion and the formanilide product are directly proportional to the concentration of HCOOH (Figure 3D). The influence of HCOOH:NB molar ratio is investigated. When the HCOOH concentration varies from 6 equivalents to 14 equivalents, the NB conversion increases linearly. Using 12 equivalents of HCOOH with respect to NB, the best result is obtained. Thus 1 mmol of NB is reacted with 12 mmol of HCOOH at 413 K for 8 h using 30 mg of $ZnCo-N@C_{(ZIF-COF)}$ to obtain the best activity. The influence of various solvents suggests that the reaction proceeds well in THF and toluene (Figure S10). Higher formanilide selectivity is obtained in toluene, which is consistent with a previous report, which suggests that higher CO is produced in toluene.^[17,45] Reaction proceeds even good in H_2O medium. However, under the optimized reaction condition, low formanilide selectivity is observed. With an increase in the

reaction temperature, the formanilide selectivity increases. This suggests that in water, up to 413 K, decarboxylation leading to $H_2 + CO_2$ is favoured over dehydration leading to $H_2O + CO$. However, above 433 K, dehydration is facilitated, and more selectivity for formanilide is obtained (Figure S11). Thus, this result clearly shows that extent of decarboxylation and dehydration depends on temperature and solvent.

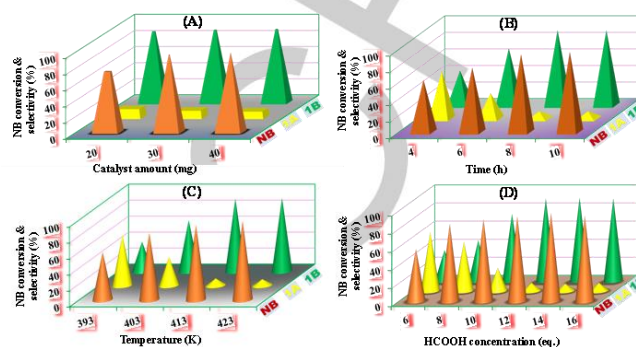
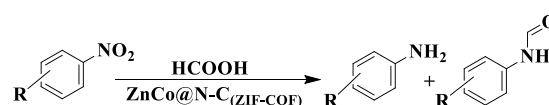


Figure 3. Influence of (A) catalyst amount, (B) reaction time, (C) reaction temperature and (D) formic acid concentration, in the reductive formylation of nitrobenzene over $ZnCo-N@C_{(ZIF-cof)}$.

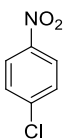
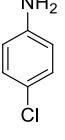
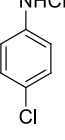
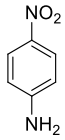
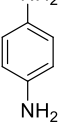
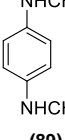
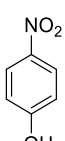
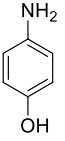
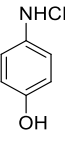
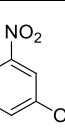
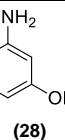
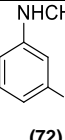
The reaction proceeds very well using substituted nitroarenes. A good to excellent conversion and N-formylated product selectivity of the substituted nitroarenes is observed (Table 3). *p*-amino nitro benzene leads to producing di N-formylated compound as a major product. No dehalogenation or demethoxylation, or dehydroxylation is observed, suggesting that selective reduction and reductive formylation take place in the presence of several functional groups. This suggests the present catalyst tolerates a wide range of functional groups and indicates the general applicability of this catalyst in reductive N-formylation of nitro compounds.

Table 3. Reductive N-formylation of nitroaromatics using HCOOH over $ZnCo-N@C_{(ZIF-cof)}$.



Entry	Reactant	Conv. (%)	Selectivity (%)	
			1a	1b
1		92	 (9)	 (91)
2		89	 (12)	 (88)

FULL PAPER

3		90	 (16)	 (84)
4		93	 (11)	 (89)
5		84	 (21)	 (79)
6		78	 (28)	 (72)

Reaction condition: Nitroarene (1 mmol), HCOOH (12 equiv.), Catalyst (30 mg), THF (7 mL), temperature (413 K), time (8 h).

The hot-filtration test was carried to substantiate the heterogeneity of the $\text{ZnCo-N@C}_{(\text{ZIF-COF})}$ catalyst (Figure S12A).^[17] The catalyst was removed after 4 h, and the reaction was continued for another 4 h in the absence of catalyst. No significant increase in NB conversion was observed, which signifies the truly heterogeneous nature of the reaction. The $\text{ZnCo-N@C}_{(\text{ZIF-COF})}$ was recycled five times in the N-formylation of NB (Figure S12B). After each run, the catalyst was filtered, washed with ethanol, and dried in a vacuum, and then used in the next cycle. No significant loss in the catalytic activity was observed after five cycles. The Co content for the spent catalyst is compared with the fresh catalyst using elemental analysis (MP-AES). A negligible loss of the cobalt content (2.5 ppm) is observed for the recovered catalyst. The spent catalyst was subjected to PXRD, Raman analysis, and TEM measurement (Figure S13). The obtained results demonstrate that the spent catalyst is stable and remains undisturbed after the recycling experiments. The I_D/I_G value did not change significantly compared to the fresh catalyst, indicating that the graphitic nature is preserved during recycling experiments.

KSCN poisoning test was conducted to justifying the role of the metallic constituents present in $\text{ZnCo-N@C}_{(\text{ZIF-COF})}$ in the N-formylation of NB. After 4 h of the reaction, KSCN was introduced in the reaction mixture. The progress of the reaction was seized because SCN^- masks and deactivates the metallic constituents present in the catalyst (Figure S14). KSCN (SCN^-) strongly interacts with the small metallic Co nanoclusters and Co-N_x species. SCN^- masks the active sites by coordinating with metal centres in the catalyst and deactivate the catalyst. Whereas the CoO_x and larger Co nanoparticles are reported to exhibit no effect with the KSCN poisoning test.^[46,48] This experiment suggests that the small nanoclusters are present in the catalyst, which further confirms the results obtained from

TEM. The catalytic poisoning test confirms that the catalytic activity is mainly due to the presence of Co-N_x and Co nanoclusters. One more control experiment was performed to overrule the possibility of CO poisoning. First, the reaction was carried out in the presence of 1 bar CO pressure, and then the recovered catalyst was subjected to a fresh catalytic run. Reaction conducted using recovered catalyst exhibits similar activity (NB conversion = 91 % and formamide selectivity = 93 %) to that of the original catalyst suggesting that CO poisoning did not occur.

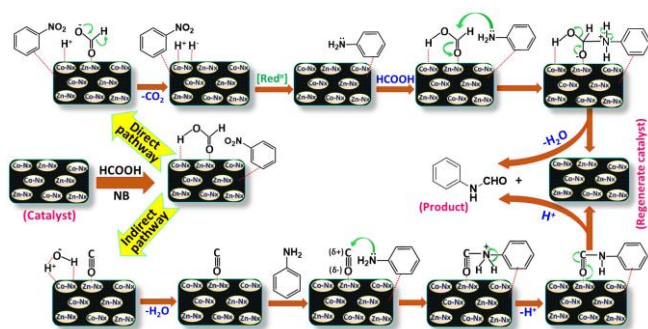
The nitrogen-rich polymer framework present in the COF template empowers the ZnCo-ZIF framework to architect a well-ordered porous architecture with high surface area and bimetallic constituent's embedded in the nitrogen-containing graphitic carbon framework upon the carbonization process. The carbonization strategy is adopted here to prepare metal nanoclusters embedded porous N-doped graphitic carbon catalyst. Using conventional carbon/nitrogen precursors, during the carbonization process, the framework shrinkage and metal agglomeration are commonly observed. Hence the resulted graphitic carbon-nitride lacks porosity and exhibits low surface area. Hard template such as silica nanoparticles or mesoporous silica has been used as a sacrificial template to overcome this problem. However, the removal of sacrificial silica template is cumbersome and hazardous process due to the involvement of a strong base or HF.^[17] Herein, COF is used as a soft-template and C-N source that entangled with ZnCo-ZIF to produce a porous framework, which upon carbonizing produces porous C-N framework with entrapment of Co and Zn nanoclusters. Such advantageous features are not obtained when melamine is used as C, N source. Thus, the $\text{ZnCo-N@C}_{(\text{ZIF-COF})}$ superior catalytic activity is due to the large numbers of dispersed active sites ($\text{Zn-N}_x/\text{Co-N}_x$) throughout the porous graphitic C-N framework. The formic acid adsorption also depends on the basicity of the catalyst. To determine the basicity of the catalyst, CO_2 -temperature-programmed desorption (CO_2 -TPD) analysis was conducted (Figure S15). The amount of desorbed CO_2 depends on the basicity and surface area of the material. The CO_2 desorbed amount follows the order $\text{ZnCo-N@C}_{(\text{ZIF-COF})} > \text{ZnCo-N@C}_{(\text{ZIF-MEL})} > \text{ZnCo-N@C}_{(\text{ZIF})}$. CO_2 -TPD profiles show that CO_2 desorbs at three different temperatures. The physisorbed CO_2 desorption occurs below 373 K, whereas the desorption in the range of 373 K - 453 K and 623 K - 723 K attributes weak and strong basic sites, respectively. The strong basic strength follows the order $\text{ZnCo-N@C}_{(\text{ZIF-COF})} > \text{ZnCo-N@C}_{(\text{ZIF-MEL})} > \text{ZnCo-N@C}_{(\text{ZIF})}$. Moreover, the suitable nitrogen environment (pyrrolic group) present in the catalyst provides stability and reactivity to Zn-N_x/Co-N_x active sites, which is responsible for the reductive N-formylation. The XPS result shows the pyrrolic N content follows the order $\text{ZnCo-N@C}_{(\text{ZIF-COF})} > \text{ZnCo-N@C}_{(\text{ZIF-MEL})} > \text{ZnCo-N@C}_{(\text{ZIF})}$. Being an acidic molecule, HCOOH ($\text{HCOOH} \rightarrow \text{H}_2, \text{CO}, \text{CO}_2$) efficiently adsorbs on the large surface area containing basic catalysts.

The NB adsorption on the catalyst surface is also an important step in the heterogeneous catalytic reaction. The NB is a UV-active molecule. Hence the extent of NB adsorption on the different catalysts was estimated using UV-Vis spectroscopy (Figure S16). Initially, 100 ppm concentration of an ethanolic solution of NB was taken with 20 mg of the catalyst. After 1 h of equilibration, the liquid part was withdrawn and evaluated under UV-Vis spectroscopy. The NB concentration in the solution was decreased (as shown in Figure S16), which confirms the

FULL PAPER

adsorption of NB at the catalyst surface. Thus, the NB adsorption, optimum basicity, N-environment & contents, and effective entrapment of highly dispersed metal nanoclusters are responsible for the excellent activity of ZnCo-N@C_(ZIF-COF).

After evaluating the catalytic data, control reactions, and physicochemical properties, a plausible mechanism for the reductive N-formylation of the NB is proposed. HCOOH and NB adsorb in close proximity at the surface of ZnCo-N@C_(ZIF-COF) catalyst. The Zn-Nx sites and the C-N framework facilitate the HCOOH adsorption process by Zn-formate mechanism pathway or direct pathway.^[23] This leads to the decarboxylation of HCOOH and the formation of Co-H active species, which reacts with the adsorbed NB to form adsorbed aniline via a transfer hydrogenation approach. The lone pair of nitrogen of adsorbed aniline reacts with adsorbed HCOOH, followed by dehydration to form formanilide via a direct pathway. At the same time, the dehydration/decarbonylation of HCOOH produces adsorbed CO species by an indirect pathway at Co sites. Subsequently, the aniline_{ads} and CO_{ads} react and produce formanilide and regenerate the active catalytic sites (Scheme 2).



Scheme 2. Plausible mechanism of the reductive N-formylation of nitrobenzene over ZnCo-N@C_(ZIF-COF).

Conclusion

In summary, ZnCo-MOF and COF entangled material was synthesized and carbonized to prepare ZnCo embedded N-doped porous carbon material. ZnCo embedded N doped porous carbon exhibited a very good surface area of 684 m²/g. Raman and TEM analysis confirmed that the material is graphitic. TEM analysis confirmed that the tiny nanoclusters were highly dispersed, and metal nanoparticles were not visible in the HRTEM image. Elemental mapping and XPS analysis confirmed that Zn's large content was evaporated during the carbonization process, and low content of Zn was embedded in the C-N framework. XPS analysis confirmed that Co is present in Co(0), CoO_x, and CoN_x states, and pyrrolic, pyridinic, and graphitic N were present in the C-N framework. The catalyst exhibited excellent activity in the selective reductive N-formylation of nitroaromatics using formic acid. The high surface area porous C-N framework was suitable for the adsorption of nitrobenzene. The high surface area and basic C-N framework were ideal for the adsorption of HCOOH. Moreover, Zn sites present in the catalyst facilitated the adsorption of HCOOH. By the direct formylation route, adsorbed nitrobenzene and formic acid reacted to produce formanilide. Embedded Co metals decomposed HCOOH to H₂ and CO via decarboxylation (H₂ +

CO₂) and dehydration pathway (CO + H₂O) at an optimum temperature in a suitable solvent medium in optimum ratio to produce formanilide by indirect pathway. Both paths are responsible for forming the desired reductive N-formylated product. Zn-N_x sites were active sites for HCOOH adsorption, and Co nanoclusters & Co-N_x were active sites for CO+H₂ generation for reductive N-formylation. The doping of Zn and Co in the form of tiny nanoclusters on a high surface area porous C-N framework will be interesting to materials scientists, and its selective reductive formylation of nitrobenzene will be attractive for catalysis researchers.

Experimental Section

Catalyst preparation

Initially, the COF was prepared using a reported method.³² A specific amount of COF was dispersed in methanol. Then, Zn(NO₃)₂·6H₂O (0.550 g) and Co(NO₃)₂·6H₂O (0.184 g) were dissolved in the dispersed solution and stirred for 2 h. After this, a 70 mL methanolic solution of 2-methyl imidazole was added and stirred for 24 h at ambient conditions. Then it was centrifuged and washed with methanol several times and dried under an oven at 343 K. The synthesized COF-ZIF composite material was carbonized at the desired temperature with a heating ramp of 5 °K min⁻¹ in an Ar atmosphere for 2 h and designated as ZnCo-N@C_(ZIF-COF). For comparison, another ZnCo-N@C was prepared by taking melamine instead of COF as support. The obtained ZnCo-N@C was designated as ZnCo-N@C_(ZIF-MEL). The support free ZnCo bimetallic ZIF was also prepared and carbonized to give ZnCo-N@C_(ZIF). The details of instruments used for the catalyst characterization are provided in the Supporting Information Section.

Procedure of the catalytic reactions

The procedures of the catalytic reactions discussed in this study are provided in the supporting information section.

Acknowledgments

Authors are grateful to SERB New Delhi (CRG/2020/000028) and the Director IIT Ropar for the Mid-career Excellency in the Research through grant number 9-35/2009/IITRPR/3121. AKK thanks MHRD for Senior Research Fellowship.

Conflicts of interest

The authors declare no competing financial interest.

Keywords: Selective reductive formylation • N-Formylation • MOF • COF • C-N framework.

Supporting Information

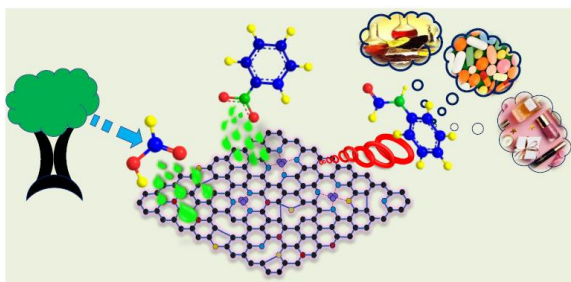
The details for the catalytic reactions, activation energy determination, and some catalytic activity data and physicochemical characterization are provided in the Supporting Information section. Supporting information also includes

FULL PAPER

material characterization, and steps involved in catalytic reactions, XRD, FE-SEM, catalyst recyclability, optimization of reaction parameters, adsorption experiments data, and CO₂-TPD data.

- [1] M. M. Khin, A. S. Nair, V. J. Babu, R. Murugan, S. Ramakrishna, *Energy Environ. Sci.*, **2012**, *5*, 8075–8109.
- [2] W. F. Hoelderich, *Catal. Today*, **2000**, *62*, 115–130.
- [3] B. Johnston, M. C. Mayo, A. Khare, *Technovation*, **2005**, *25*, 569–585.
- [4] M. D. Porosoff, B. Yan, J. G. Chen, *Energy Environ. Sci.*, **2016**, *9*, 62–73.
- [5] A. K. Kar, S. P. Kaur, T. J. D. Kumar, R. Srivastava, *Catal. Sci. Technol.*, **2020**, *10*, 6892–6901.
- [6] I. Staffell, D. Scamman, A. V. Abad, P. Balcombe, P. E. Dodds, P. Ekins, N. Shahd and K. R. Warda, *Energy Environ. Sci.*, **2019**, *12*, 463–491.
- [7] C. S. Martavaltzi, E. P. Pampaka, E. S. Korkakaki, A. A. Lemonidou, *Energy Fuels*, **2010**, *24*, 2589–2595.
- [8] P. Parthasarathy, K. S. Narayanan, *Renewable Energy*, **2014**, *66*, 570–579.
- [9] Z. Wang, R. R. Roberts, G. F. Naterer, K. S. Gabriel, *Int. J. Hydrogen Energy*, **2012**, *37*, 16287–16301.
- [10] Y. Wang, S. Zhang, *Energy Sources Part B: Econ. Plan Policy*, **2017**, *12*, 1022–1029.
- [11] M. J. Gilkey, B. Xu, *ACS Catal.*, **2016**, *6*, 1420–1436.
- [12] D. Wang, D. Astruc, *Chem. Rev.*, **2015**, *115*, 6621–6686.
- [13] K. Fang, D. Li, M. Lin, M. Xiang, W. Wei, Y. Sun, *Catal. Today*, **2009**, *147*, 133–138.
- [14] M. Mahmudzadeh, H. Yari, B. Ramezanzadeh, M. Mahdavian, *J. Hazard. Mater.*, **2019**, *371*, 609–624.
- [15] Q. L. Zhu, Q. Xu, *Energy Environ. Sci.*, **2015**, *8*, 478–512.
- [16] F. Valentini, V. Kozell, C. Petrucci, A. Marroccoli, Y. Gu, D. Gelman, L. Vaccaro, *Energy Environ. Sci.*, **2019**, *12*, 2646–2664.
- [17] A. K. Kar, R. Srivastava, *ACS Sustainable Chem. Eng.*, **2019**, *7*, 13136–13147.
- [18] J. Reichert, J. Albert, *ACS Sustainable Chem. Eng.*, **2017**, *5*, 7383–7392.
- [19] P. Zhou, Z. Zhang, L. Jiang, C. Yu, K. Lv, J. Sun, S. A. Wang, *Appl. Catal., B*, **2017**, *210*, 522–532.
- [20] B. C. Chen, M. S. Bednarz, R. Zhao, J. E. Sundeen, P. Chen, Z. Shen, A. P. Skoumbourdis, J. C. Barrish, *Tetrahedron Lett.*, **2000**, *41*, 5453–5456.
- [21] D. N. Sawant, Y. S. Wagh, K. D. Bhatte, B. M. Bhanage, *J. Org. Chem.*, **2011**, *76*, 5489–5494.
- [22] B. B. Lohray, S. Baskaran, B. S. Rao, B. Y. Reddy, I. N. Rao, *Tetrahedron Lett.*, **1999**, *40*, 4855–4856.
- [23] M. Nasrollahzadeh, N. Motahharifar, M. Sajjadi, A. M. Aghbolagh, M. Shokouhimehr, R. S. Varma, *Green Chem.*, **2019**, *21*, 5144–5167.
- [24] L. Mámáni, M. Sheykhan, A. Heydari, M. Faraji, Y. Yamini, *Appl. Catal. A*, **2010**, *377*, 64–69.
- [25] M. G. Mura, L. D. Luca, G. Giacomelli, A. Porcheddu, *Adv. Synth. Catal.*, **2012**, *354*, 3180–3186.
- [26] J. J. Sims, C. A. O. Hamou, R. Reocreux, C. Michel, J. B. Giorgi, *J. Phys. Chem. C*, **2018**, *122*, 20279–20288.
- [27] H. S. Inglis, D. Taylor, *J. Chem. Soc. A*, **1969**, 2985–2987.
- [28] M. Li, F. Xu, H. Li, Y. Wang, *Catal. Sci. Technol.*, **2016**, *6*, 3670–3693.
- [29] K. Shen, X. Chen, J. Chen, Y. Li, *ACS Catal.*, **2016**, *6*, 5887–5903.
- [30] W. Yang, X. Li, Y. Li, R. Zhu, H. Pang, *Adv. Mater.*, **2019**, *31*, 1804740–1804775.
- [31] A. K. Kar, R. Srivastava, *Inorg. Chem. Front.*, **2019**, *6*, 576–589.
- [32] M. G. Schwab, B. Fassbender, H. W. Spiess, A. Thomas, X. Feng, K. Mullen, *J. Am. Chem. Soc.*, **2009**, *131*, 7216–7217.
- [33] G. L. Zhuang, Y. F. Gao, X. Zhou, X. Y. Tao, J. M. Luo, Y. J. Gao, Y. L. Yan, P. Y. Gao, X. Zhong and J. G. Wang, *Chem. Eng. J.*, **2017**, *330*, 1255–1264.
- [34] X. Xu, S. Zhang, J. Tang, L. Pan, M. Eguchi, J. Na, Y. Yamauchi, *Energy Chem.*, **2020**, *2*, 100043–100076.
- [35] J. Tan, X. He, F. Yin, B. Chen, X. Liang, G. Li, H. Yin, *Int J Hydrogen Energy*, **2020**, *45*, 15453–15464.
- [36] X. Zhao, N. Yan, *RSC Adv.*, **2015**, *5*, 69955–69961.
- [37] K. Sun, S. Chen, J. Zhang, G. P. Lu, C. Cai, *ChemCatChem*, **2019**, *11*, 1264–1271.
- [38] J. Xue, Y. Li, J. Hu, *J. Mater. Chem. A*, **2020**, *8*, 7145–7157.
- [39] Y. Zhang, P. Cao, H. Y. Zhang, G. Yin, J. Zhao, *Catal. Commun.*, **2019**, *129*, 105747.
- [40] X. Lan, B. Ali, Y. Yang, T. Yang, *ACS Appl. Mater. Interfaces*, **2020**, *12*, 3624–3630.
- [41] Y. Wu, Z. Chen, W. C. Cheong, C. Zhang, L. Zheng, W. Yan, R. Yu, C. Chen, Y. Li, *Chem. Sci.*, **2019**, *10*, 5345–5352.
- [42] Y. Su, Y. Zhu, H. Jiang, J. Shen, X. Yang, W. Zou, J. Chen, C. Li, *Nanoscale*, **2014**, *6*, 15080–15089.
- [43] E. Jerero, J. M. Vohs, *Catal. Lett.*, **2009**, *130*, 271–277.
- [44] D. A. Bulushev, M. Zacharska, S. Beloshapkin, Y. Guo, I. Yuranov, *Appl. Catal. A*, **2018**, *561*, 96–103.
- [45] F. Chen, B. Sahoo, C. Kreyenschulte, H. Lund, M. Zeng, L. He, K. Junge, M. Beller, *Chem. Sci.*, **2017**, *8*, 6239–6246.
- [46] C. Tang, A. E. Surkus, F. Chen, M. M. Pohl, G. Agostini, M. Schneider, H. Junge, M. Beller, *Angew. Chem.*, **2017**, *129*, 16843–16847.
- [47] N. Ishito, K. Hara, K. Nakajima, A. Fukuoka, *J Energy Chem.*, **2016**, *25*, 306–310.
- [48] M. Li, S. Chen, Q. Jiang, Q. Chen, X. Wang, Y. Yan, J. Liu, C. Lv, W. Ding, and X. Guo, *ACS Catal.*, **2021**, *11*, 3026–3039.

Insert graphic for Table of Contents here. ((Please ensure your graphic is in **one** of following formats))



Insert text for Table of Contents here. ((Reactants adsorption, optimum basicity, N-environment & contents, and effective entrapment of highly dispersed metal nanoclusters are responsible for the excellent activity of ZnCo-N@C_(ZIF-COF) in the reductive N-formylation of nitroaromatics to corresponding formamides as potential precursors.))